Chapter 14
The Measurement of Thermally Stimulated Depolarization and Polarization Currents

M. P. F. Graça and P. R. Prezas

Abstract The measurement of thermally stimulated depolarization currents, a technique usually known by its initials (TSDC), has contributed substantially to the knowledge and understanding of charge storage and charge decay processes in several types of electret materials, i.e., materials that can have electrical polarization arising from kinetically trapped charges. The polarization of these materials may increase the magnitude of the applied electric field, until the point of dielectric breakdown. A similar, and sometimes complementary, technique consists in the measurement of thermally stimulated polarization currents (TSPC). This contribution discusses experimental and theoretical considerations regarding both techniques. Additionally, it also includes a case study regarding $LiNbO_3$ glass-ceramics, synthesized by the melt-quenching process.

Keywords TSDC · TSPC · $LiNbO_3$ · Glasses · Glass-ceramics

14.1 Introduction

The measurement of thermally stimulated depolarization and polarization currents, TSDC and TSPC, respectively, are part of a broad group of thermally stimulated experimental techniques, where a given physical property of the material is studied as a function of the temperature. In the cases of TSDC and TSPC the property in analysis, i.e., the electric current, is strictly related to dipolar polarization/depolarization and spatial charge detrapping/decay processes activated by both the temperature and the applied electric field.

The designation TSDC does not coincide with the appearance of this technique in the scientific community, which occurred in 1964 when it was introduced by Bucci and collaborators [1]. The technique was introduced under the designation ionic

M. P. F. Graça (✉) · P. R. Prezas
I3N and Physics Department, University of Aveiro, Aveiro, Portugal
e-mail: mpfg@ua.pt

thermoconductivity ITC, because it would be applied in the analysis of ion related processes such as dipolar relaxation, among others. The terminology TSDC was posteriorly adopted to include materials where both ionic and electronic charges yield a significant contribution to the magnitude of the polarization and the respective depolarization or polarization currents [2]. TSDC and TSPC have found a substantial amount of applications in the study of the electrical properties of glasses, glass-ceramics, and polymers [3, 4]. However, since the charge transport and trapping processes are not only essential for electrets, they have also found significant applications in the characterization of materials applied as thin films, such as photoconductors and electro-optic devices [5]. Additionally, features such as the very high sensitivity (capable of detecting small contributions to the polarization, due to dipole densities on the order of 10^{15} dipoles per cubic centimeter) and the resolving power contributed to the popularization of these techniques. Furthermore, the theoretical description and following mathematical formulation of the different processes contributing to the depolarization currents are already well established.

The present contribution is divided into two main sections: the first deals with the theoretical and experimental characteristics of both techniques, while the second will contain a case study regarding TSDC measurements on $LiNbO_3$ and $NaNbO_3$ containing glasses and glass-ceramics, synthesized by melt-quenching and sol-gel processes.

14.2 Background

14.2.1 TSDC: Thermally Stimulated Depolarization Currents

The experimental details and steps of the TSDC technique are directly related to the fact that when heating up a solid dielectric material which is electrically polarized through the application of an external dc electric field, the relaxation time of the sample's polarizable components will be small enough so that the polarization reaches its saturation condition in a short period. If the electric field is kept applied while the sample temperature is decreased down to a temperature low enough so that the relaxation times are very high, the polarization can be considered as "frozen". At this point, it will remain "frozen" even after the removal of the electric field, since the thermal energy is not high enough to activate the return of the charge carriers to their equilibrium positions. If the temperature of the sample is again increased, there will be a gradual release of the trapped charges, originating a depolarization current.

This process, represented schematically in Fig. 14.1, is based on the execution of the following experimental steps [6, 7]:

1. Application to the sample (with appropriate electrodes), at a polarization temperature T_p, of an electric dc field E_p during a period t_p high enough so that the polarization reaches its saturation condition.

Fig. 14.1 Scheme of a
typical TSDC experiment
[9]
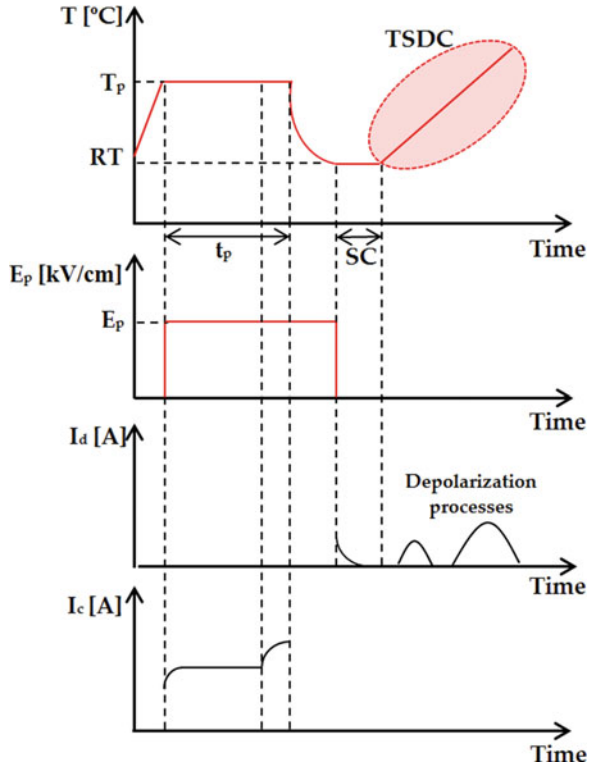
2. The sample is cooled, preferably with a high cooling rate while keeping the field
   E_p applied, down to a temperature T_0 where the dipolar motions can be regarded
   as negligible.
3. E_p is removed, and the sample is short-circuited (SC step in Fig. 14.1) for a few
   minutes to release weakly bonded charges.
4. The sample is connected to a very sensible electrometer (currents as low as 10^{-15}
   A may be detected) and warmed up with a constant heating rate β. The depolar-
   ization current is measured as function of the temperature. The origin of this
   current is the relaxation of the charge carriers.

   Figure 14.1 also depicts the behavior of the charge current I_c and the current
discharge I_d. As expected, the charge current increases during the time of E_p
application, reaching a saturation condition. During the SC step, a discharge current
can be detected, related to the release of weakly bonded charges. Subsequently, the
depolarization processes will be detected as currents in the I_d versus
temperature plot.
   As the most significant advantages of this technique, we highlight [3, 8]:

1. In materials with multiple relaxation processes, each process should originate a
   separated TSDC current peak.

2. It does not require an applied external electric field during the measurements, decreasing by this way the electric conduction effects.
3. Allows making quantitative measurements of: impurities concentration; molecular movements; characterization of macromolecular states; local environment characterization; chemical degradation; structural anisotropy.

As main disadvantages of this technique, the high sensibility and resolution required for the data acquisition system can be stated.

Taking into account the discussed experimental procedure, it is clear that all TSDC measurements will need some mandatory equipment. The list contains a furnace or cryostat, depending on the temperature range to analyze, a temperature controller capable of controlling a linear variation of the temperature as a function of time, with high-precision, a stable dc power supply for the electrical polarization and a sensible electrometer. Depending on the sample or type of measurement intended, a vacuum container and the possibility of controlling the atmosphere may be desirable. In conclusion, Fig. 14.2 shows a general setup for a TSDC measurement, with all the equipment that was referred to.

14.2.2 TSDC: Physical Processes and Mathematical Formulation

It is known that different processes can contribute to the measured depolarization current of a given sample. Among theseprocesses, the followingcan be highlighted:
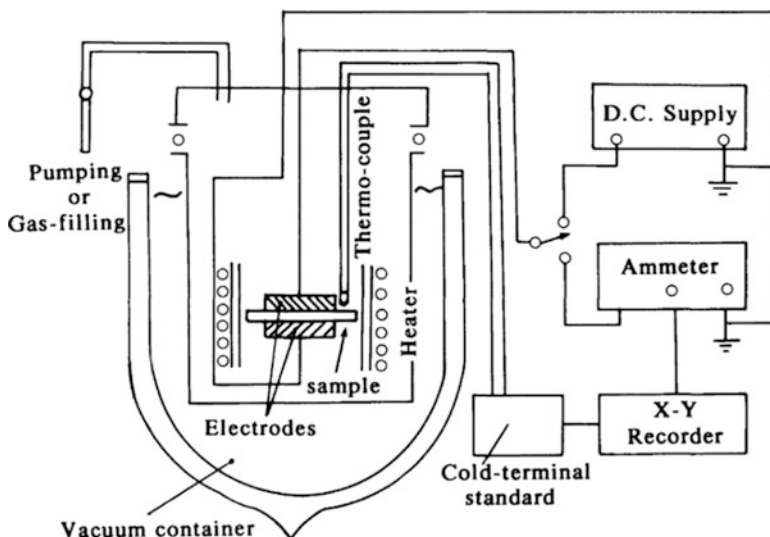

Fig. 14.2 General experimental setup for a TSDC experiment [10]

the reorientation of electric dipoles (dipolar polarization), the movement of trapped electric charges, i.e., space charge detrapping, the displacement of the electronic cloud within an atom or ion (induced electronic polarization) or the ionic displacement within a molecule (induced dipolar polarization), the formation of defect dipolar polarization, etc. [2, 10].

The analytical expressions describing the depolarization current are usually applied in materials where ionic processes dominate the response, i.e., the electronic response can be considered negligible. In such a case, two formulations are most commonly used, for dipolar reorientation and space charge detrapping processes, respectively. For a depolarization current peak originated from dipolar reorientation, and a first order process, the dependence of the current density on the temperature [J (T)] is given by Eq. 14.1 [2, 10, 11]:

$$J(T) = \frac{P_0}{\tau_0} \exp\left[-\frac{E_a}{k_B T}\right] \exp\left[-\frac{1}{\beta}\exp\left(\int_{T_0}^{T} \tau(T)d(T)\right)\right] \qquad (14.1)$$

where P_0 is the equilibrium polarization (basically, the sample's polarization before starting the measurement), τ_0 is a pre-exponential factor that can be interpreted as the relaxation time when the temperature tends to infinite, E_a is the activation energy for dipole relaxation/reorientation, k_B is Boltzmann constant, β the heating rate and $\tau(T)$ the characteristic relaxation time. For dipolar reorientation, Eq. (14.1) can be modified to include an analytical expression describing the dependency of P_0 on the electric dipole density N, the individual dipole moment p, the electric field E_p, and the polarization temperature T_p, yielding the following expression [2, 10, 11]:

$$J(T) = \frac{Np^2 E_p}{3k_B T_p \tau_0} \exp\left[-\frac{E_a}{k_B T}\right] \exp\left[-\frac{1}{\beta}\exp\left(\int_{T_0}^{T} \tau(T')d(T')\right)\right] \qquad (14.2)$$

Equation 14.2 is usually labeled as Bucci-Fieschi theory, describing a depolarization current peak due to a dipolar reorientation process.

On the other hand, to describe a peak originating from spatial charge detrapping, the Bucci-Fieschi can be still applied to describe the depolarization of space charge, assuming that all the trapped charges have approximately the same mobility. In this case, the equilibrium polarization P_0 is given by (14.3) [12]:

$$P_0 = 2qLvNt_p\exp\left(-\frac{E_a}{k_B T}\right)\sinh\left(\frac{qLE_p}{2k_B T_p}\right) = P_{SC}\sinh\left(\frac{qLE_p}{2k_B T_p}\right) \qquad (14.3)$$

where q is the ionic charge, L is the ionic jump length, v is the jump frequency, N is the density of trapped charge, t_p is the polarization time (as shown in Fig. 14.1) and E_a is the activation energy required for detrapping the charge carriers.

The mathematical treatment of Eq. (14.2) is not trivial, the main problem being the fact that the integration leads to an infinite series converging to infinite. Therefore, some approximations are needed to be considered. One of these approximations is particularly useful for the activation energy calculation: the initial rise method, introduced by Garlick and Gibson [13], is based on the fact that the integral

is negligible for temperatures lower than the peak temperature. Therefore, the equation can be simplified, and the activation energy can be evaluated through an Arrhenius dependency, as expressed in (14.4) [13] (where A is a constant):

$$J(T) = A\exp\left[-\frac{E_a}{k_B T}\right] \tag{14.4}$$

14.2.3 TSPC: Thermally Stimulated Polarization Currents

The measurement of thermally stimulated polarization currents (TSPC) is a counterpart of TSDC, and also often regarded as an inverse of TSDC. TSPC involves the measurement of the current that flows through a solid dielectric material subjected to a dc electric field as the material temperature is increased with a linear rate, from some low-temperature T_0 [6]. Therefore, in TSPC there is no necessity to polarize the material previously.

Figure 14.3 shows a scheme of a typical TSPC measurement. Initially, small and current contributions may be detected due to induced dipolar and electronic polarization. These induced polarizations are typically those that respond faster to an applied electric field, due to the small distances of displacement and also, in case of the induced electronic polarization, due to the low mass of electrons. Subsequently, as temperature linearly increases, the alignment of the dipoles or other processes will be detected as currents peaks in a current versus temperature representation [14]. The


Fig. 14.3 Scheme of a typical TSPC experiment. The background current $J_B(t)$ and a dipolar contribution to the polarization current, $J_D(t)$, are also represented
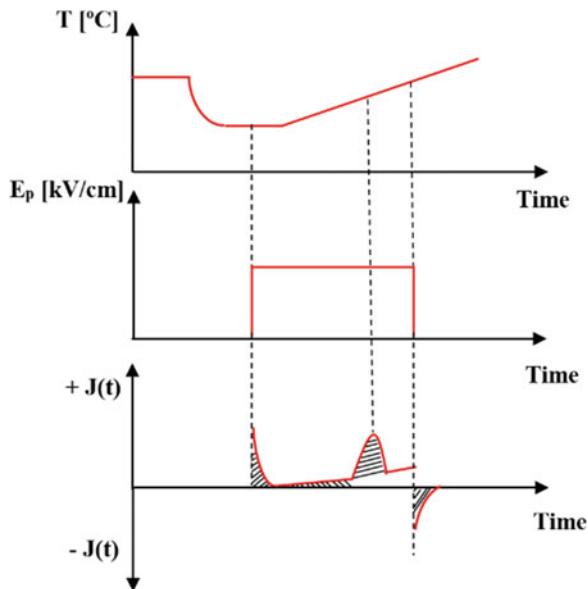
reason behind the fact of TSCP being regarded as an inverse of TSDC is that while in TSDC the current peaks are caused by the depolarization processes, in TSPC they are due to thepolarization. It is also visible in Fig. 14.3 that a background current $J_B(t)$ is detected, which is also characteristic in TSDC measurements. $J_D(t)$ represents the dipolar contribution of the measured current. About the additional/complementary information that TSPC can provide, the possibility is highlighted to distinguish the physical process behind dipolar depolarization processes observed in TSDC spectra. While depolarization peaks related to dipolar reorientation will be centered at about the same temperature in both TSDC and TSPC spectra, but with opposite direction, processes related to vacancies and impurities diffusion will be detected as an exponential rise of the current in the TSPC spectrum. Figure 14.4 shows this behavior for a $BaF_2:Tb^{3+}$ single crystal [15]. While the first process at about 195 K is caused by the reorientation of $F-Tb^{3+}$ dipoles, the second at around 340 K is assigned to the diffusion of fluoride vacancies, therefore it is detected as an exponential rise of the current. It is to be noted that the mathematical formulas for both techniques is essentially the same, i.e., the formulations discussed in the TSDC section are the same for both techniques, the only difference being that T_p has to be replaced by a variable temperature T.

The equipment required for TSPC measurements is essentially the same as described for TSDC. However, one of the reasons that explain the fact of TSDC being the most popular technique is that the signal to noise ratio in a current measurement is markedly better if the current is measured without an applied electric field.

Fig. 14.4 Recorder plots of TSPC (above) and TSDC (below, designated as ITC – ionic thermo-conductivity) measurements performed with a $BaF_2:Tb^{3+}$ single crystal [15]
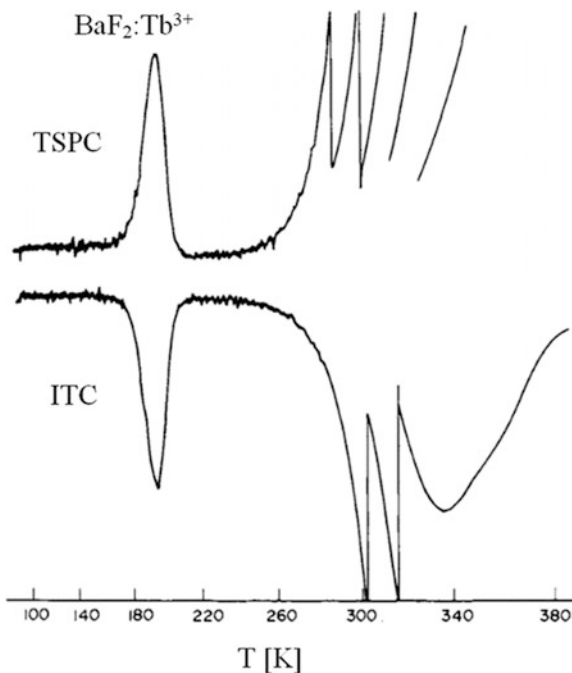
14.3   Case Study: Glass and Glass-Ceramics with LiNbO₃

Glass refers to one of the oldest known materials of mankind. It is defined, according to ASTM C-169-92, as a inorganic product obtained by rapid cooling of a melt, to conditions of rigidity, without crystallization. This definition is, however, too restrictive as it only applies to glasses prepared by the fusion method. A broader definition was proposed by A. Paul [16]: glasses possess the elastic behavior characteristic of the crystalline state and the viscous behavior of the liquid state. The most common properties of vials are transparency to visible radiation, mechanical stability, inactivity at the biological level and electrical insulation. However, due to the possibility of controlling the microstructure either by altering the initial composition or by application of heat treatments, controlling the nucleation and crystallization process [17, 18], the properties of a glass can be modified.

The initial chemical composition is a controllable factor that allows to mold some of the properties of the glass. In any glass, the units that define its structure can be divided into three categories, according to their structural function: network former,; modifier, and intermediate units. The network formers are those units which, that without addition of other components can form glass, such as SiO_2, B_2O_3, P_2O_5 and GeO_2. The network modifier do not form glass structures but are often combined with a former. Examples of modifying elements are the alkali elements (Li, Na, K, etc.) and the alkaline earth metals (Mg, Ca, etc.). The intermediate species are elements that can either have the role of the network former or the modifier (Al, Nb, etc.).

The formation of glass ceramics, for example by heat treatment of the base glass, is technologically advantageous for monocrystals and sintered ceramics. It gives the possibility to control their properties (optical, electrical, mechanical, chemical, etc.) by the volumetric fraction of the active phase dispersed in the matrix [19]. For example, to maintain optical transparency, the nucleation and crystal growth process require high control; it is achieved when the size of the crystals dispersed in the glass matrix is not high enough to cause light scattering. However, for most electrical applications it is necessary that the crystals are of sufficient size to have, for example, a ferroelectric response. This commitment is not easy to meet. Another condition which can maintain the optical transparency of a ceramic glass is a small difference between the refractive indexes of crystals and glass matrix. If this difference is insignificant, it allows, regardless of the size of the crystals, to maintain the optical transparency of the ceramic glass [20]. Thus, in recent years there has been a growing interest in the preparation, characterization and technological implementation of glass and ceramics. However, it is important to note that in general the electrical and optical properties of ceramic glasses are not as good as those of monocrystals. This is because ceramics show at least two distinct phases, a crystalline (considered the active phase) and anamorphous (support). The electrical polarization of the crystals inserted in a glassy matrix is hampered due to the low value of the dielectric constant of the glassy phase [21, 22]. On the other hand, as the growth processes of monocrystals have a high economic cost, they are now judged deprecated forceramic glasses. Some of these also have the advantage of being dense materials with no porosity [23].

Different processes can achieve crystalline growth with preferred orientation, for example: mechanical deformation; thermodynamic control; kinetic control (induced electrochemical nucleation) [18]. In glasses, the use of thermodynamic control is the most common process. However, control of crystallization with the desired crystalline phase is usually difficult as crystallization is a complex process and affected by various factors such as composition, surface conditions, and heat treatment profiles [24].

Ceramic glasses containing ferroelectric crystals are a class of materials with high technological interest as ferroelectric crystals present a structural anisotropy that results in the formation of electric dipoles and consequently a spontaneous electrical polarization [20, 25, 26]. A large part of the ferroelectric materials is in the form of crystalline ceramics. The scientific and technological development of photonicsrequires new materials that with characteristics such as optical transparency and also optical activity to be used as amplifiers in communication systems, energy, instrumentation, etc. In this way, the preparation, and the structural, electrical and optical characterization of ceramic glasses with ferroelectric properties is of great importance for possible technological applications.

Of the various ferroelectric materials, lithium niobate ($LiNbO_3$), synthesized for the first time in 1949 by Matthias and Remeika [25], has attracted more attention from many researchers because of its excellent piezoelectric, electroacoustic, pyroelectric and photorefractive properties. In the late 1960s, due to the appearance and development of optical fiber applications, several research centers, namely the Bell Laboratories [27], studied in detail the structural characteristics and properties of $LiNbO_3$ crystals, especially their electro-optical properties [28].

The fact that $LiNbO_3$ monocrystals prepared by the usual growth techniques are a challenging and expensive task, arose the scientific interest in the structural, optical and electrical study of glass-ceramics containing $LiNbO_3$ crystals, due to the possible technological applications that can be of interest.

A significant amount of research work in the field of the preparation and crystallization of glass-ceramics containing $LiNbO_3$, by melting quenching exists. In 1980, Prasad et al. [29] published a study on the preparation of ceramic glasses from the SiO_2-Li_2O-Nb_2O_5 system. The choice of SiO_2 as a network former was due to the fact that it does not contain cations that could alter the crystalline structure of $LiNbO_3$. SiO_2 satisfies this condition due to the reduced atomic radius and coordination number. Obtaining crystals without crystalline phases is achieved for a molar amount of SiO_2 between 32% and 39%, using the same molar amount of Li_2O and Nb_2O_5.

The vitreous glass-forming region of the system (SiO_2-Al_2O_3)-Li_2O-Nb_2O_5, using the melt-quenching method, was presented by Todorovic et al. [30]. They found that ifthe molar ratio [Nb_2O_5]/[SiO_2] >1 and the molar amount of [Li_2O] >25% is, transparent and homogeneous glasses can be obtained. The application of thermal treatments to the base glass allowed the crystallization of $LiNbO_3$ particles with a size of 150–350 nm, maintaining transparency. These glass-ceramics have a refractive index of 1.84–1.93 and a dielectric constant of 155–185, measured at

1 kHz and room temperature. They observed that an increase in temperature and/or thermal treatment time leads to an increase in particle size and consequent opacity of the samples.

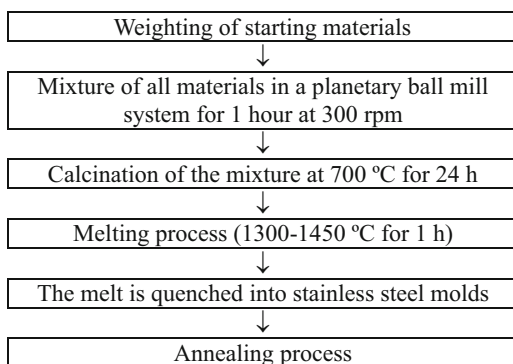## 14.4   Glass and Glass-Ceramics Preparation (Composition $60SiO_2$-$30Li_2O$-$10Nb_2O_5$ mol%)

The melt-quenching method was used to prepare transparent glasses of the ternary system SiO_2-Li_2O-Nb_2O_5. The high-purity (>99.9%) raw materials used were silicon oxide (SiO_2-BDH), lithium carbonate (Li_2CO_3-Merck) and niobium pentoxide (Nb_2O_5-Merck). The preparation of the base glass followed the procedure outlined in Fig. 14.5. The calcination step aimed to remove the CO_2 present in Li_2CO_3, thus obtaining Li_2O. The last step, the re-baking of the glass, carried out soon after the melt has been poured into the molds, has the objective of minimizing the tensions of the glass network to avoid rupture. The parameters temperature and time of calcination, temperature, melting time and temperature, and time of heat treatment (annealing) are characteristic of each system.

The base glasses were subjected to heat treatments after the annealing step to obtain ceramic glass with the crystalline phase $LiNbO_3$. Figure 14.6 represents the schematic of the thermal treatment profile used, which was carried out in a horizontal tubular furnace. The value of the threshold temperature parameter T_p is determined based on information about the glass thermal behavior.

It is important to note that prior to the heat treatment, it was necessary to polish each sample to place them with a thickness of approximately 1 mm and with the opposite surfaces as parallel as possible. Figure 14.7 shows the macroscopic appearance of the base sample and the samples heat-treated at 600 and 650 °C. It was observed that with increasing the treatment temperature the samples became in the first phase translucent and for treatments at 700 °C opaque.

Figure 14.8 shows the macroscopic appearance of the base glass in the presence of an external electric field. From the analysis of the macroscopic results, there is a

Fig. 14.5 Scheme for the preparation of base glass by the melt-quenching method

Weighting of starting materials
↓
Mixture of all materials in a planetary ball mill system for 1 hour at 300 rpm
↓
Calcination of the mixture at 700 ºC for 24 h
↓
Melting process (1300-1450 ºC for 1 h)
↓
The melt is quenched into stainless steel molds
↓
Annealing process

maximum electric field value that can be applied without modifying or even destroying the glass network. It is also noted that the presence of the electric field causes to the surface in contact with the negative electrode to have a different appearance from that which was with contact with the positive one, i.e., on the surface which was in contact with the positive electrode a white "film" is formed.

In Figs. 14.9, 14.10, and 14.11 TSDC spectra of the base glass and thermally at 600 and 650 °C treated samples, respectively, are shown. For a better visualization of the spectra, an enlargement of the low-temperature range is presented in each figure. All samples were polarized at 350 K for 10 min, applying an electric field of 50 kV/m.
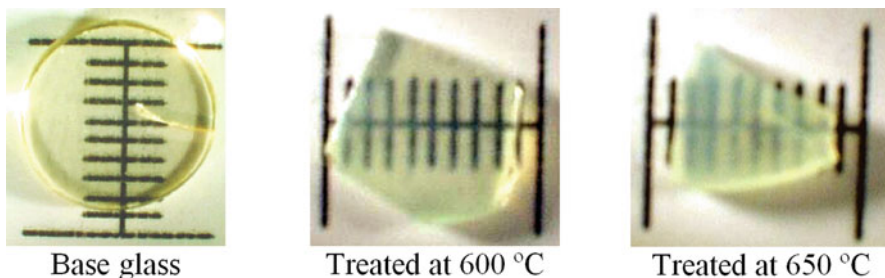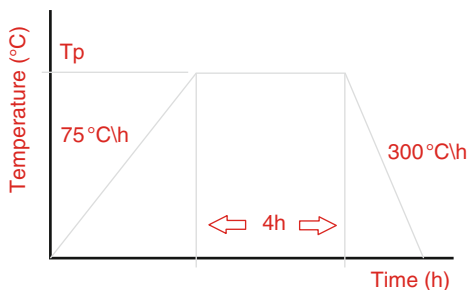
Fig. 14.6 Scheme of the heat treatment process

Base glass   Treated at 600 °C   Treated at 650 °C

Fig. 14.7 Photographs of the base glass and thermally treated samples at 600 and 650 °C (smaller scale range = 1 mm)
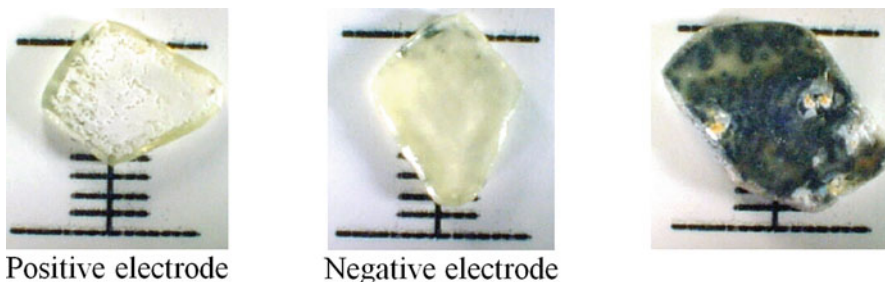

Positive electrode   Negative electrode

Fig. 14.8 Photographs of the base glass after thermal cycle in the presence of an external electric field (smaller scale range = 1 mm)
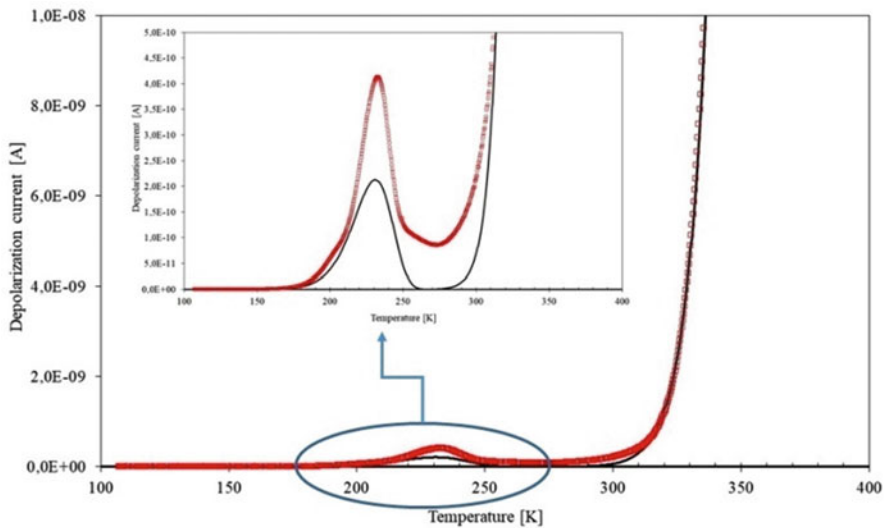
Fig. 14.9 Depolarization current as a function of the measuring temperature, for the base glass. For better visualization the inset figure shows the depolarization current at low temperatures
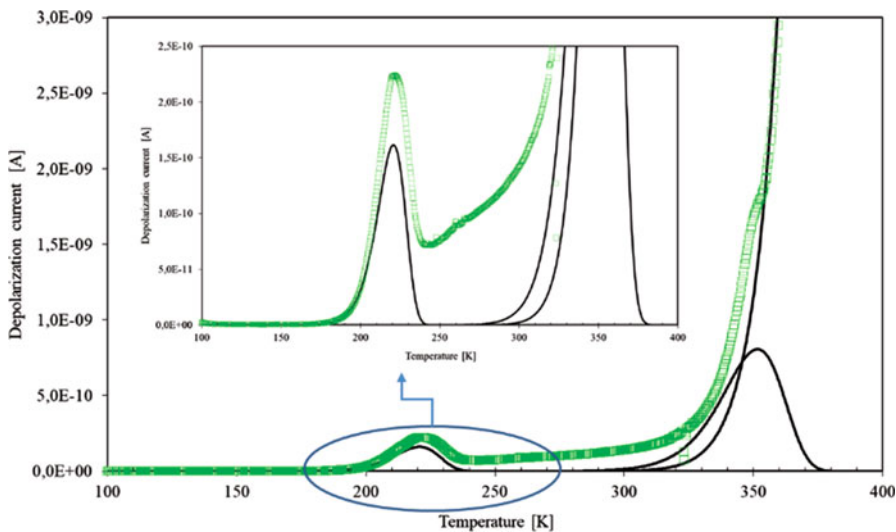

Fig. 14.10 Depolarization current as a function of the measuring temperature for the glass treated at 600 °C. For better visualization the inset figure shows the depolarization current at low temperatures
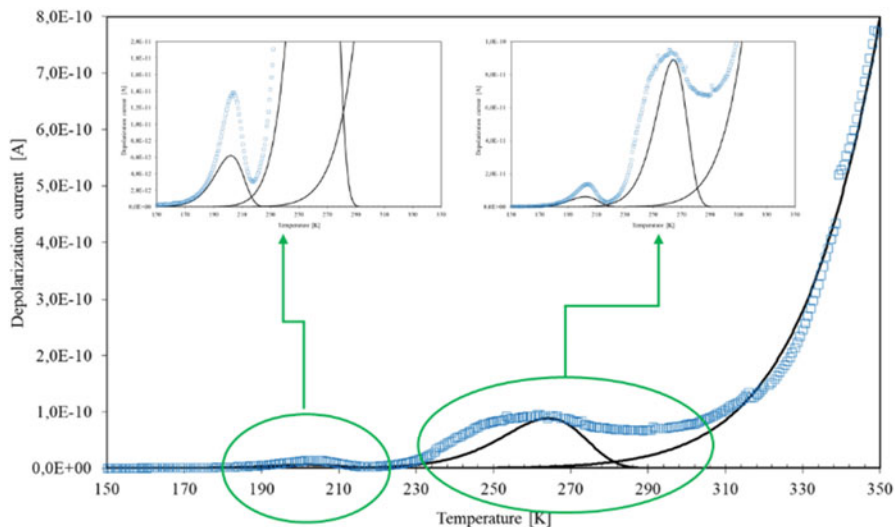
Fig. 14.11 Depolarization current as a function of the measuring temperature for the glass treated at 650 °C. For better visualization the inset figure shows the depolarization current at low T

The base glass only shows a peak of thermally active depolarization current, whereas the samples thermally treated possess two peaks, one at temperatures below ~230 K and the second at temperatures greater than 290 K. The characteristics of these peaks are listed in Tables 14.1, 14.2, and 14.3. It is observed that the temperature of the current peak in the low and high-temperature zones moves to lower temperatures with increasing heat treatment temperature. The absolute current value of both peaks also decreases from the base glass to the sample treated at 650 °C.

The activation energy E_a for each peak, calculated using the initial rise method is registered in the following tables. For the depolarization current peak at low temperatures P_1, a maximum of E_a is observed for the sample treated at 600 °C. In the high temperature zone, where the second peak P_2 is detected, there is a decrease of the correspondent E_a from the sample treated at 600 to the one at 650 °C. The relaxation time τ, associated with P_1, decreases from the base glass to the sample treated at 600 °C, but increases for the sample treated at 650 °C. For the depolarization peak P_2, the relaxation time decreases with the increase of the thermal treatment temperature.

The TSDC results of this $60SiO_2$-$30Li_2O$-$10Nb_2O_5$ %mol glass composition revealed the presence of two depolarization current peaks P_1 and P_2 in the thermally treated samples and only one depolarization peak in the base glass (P_1). The first peak P_1 is due to localized free-ion motions within the glass network. These motions give rise to a dipole orientation formed by the ion structurally inserted in the glass network (Li^+ and/or Nb^{5+}) and the non-bridge oxygen (NBO-) ion to which it is attached [31, 32]. It should be noted that in this situation the ion structurally inserted

Table 14.1 Peak temperature T_p, peak current $i_{(Tp)}$, activation energy E_a, thepre-exponential parameter $\tau_0$and the relaxation time τ, calculated for the depolarization current peak P_1, for the base glass and samples heat-treated at 600 and 650 °C

Sample	T_{P1} [K]	$i(T_{P1})$ ($\times 10^{-10}$) [A]	E_a [kJ/mol]	$\tau_{0\ (P1)}$ ($\times 10^2$) [s]	$\tau_{(P1)}$ ($\times 10^3$) [s]
Base	232.3	4.134	31.574 ± 0.198	4.159 ± 0.065	2.132
600	221.4	2.243	44.123 ± 0.265	1.262 ± 0.025	1.385
650	203.7	0.138	31.259 ± 0.151	2.626 ± 0.049	1.659

Table 14.2 Peak temperature T_p, peak current $i_{(Tp)}$, activation energy E_a,the pre-exponential parameter τ_0 and the relaxation time τ, calculated for the depolarization current peak P_2, for the samples heat-treated at 600 and 650 °C

Sample	T_{P1} [K]	$i(T_{P1})$ ($\times 10^{-10}$) [A]	E_a [kJ/mol]	$\tau_{0\ (P1)}$ ($\times 10^2$) [s]	$\tau_{(P1)}$ ($\times 10^3$) [s]
600	352.3	17.883	84.081 ± 0.959	1.044 ± 0.014	1.841
650	261.4	0.948	50.569 ± 1.843	1.646 ± 0.027	1.685

Table 14.3 Parameters of the data adjustment through the Arrhenius equation on the high-temperature measurement zone. ln(A) represents the logarithm of the pre-exponential factor, and E_a is the activation energy for the base glass and samples thermally treated at 600 and 650 °C

Sample	ln(A) [A]	E_a [kJ/mol]
Base	22,928	$115,775 \pm 0,637$
600	16,609	$108,232 \pm 0,936$
650	−3621	$80,431 \pm 0,605$

in the glass network, is not in the most favorable energetical position. According to Agarwal et al. [33], the application of an electric field results in an ion transfer towards the field thus creating electrical heterogeneity, i.e., electrical dipoles. With increasing temperature, these ions tend to return to their initial position thus creating a depolarization current that will give rise to the low-temperature peak P_1. The activation energy, associated with the origin of the electrical dipoles formed by the ions structurally inserted in the glass network, basically consists of the energy required for the movement of those ions to different positions within the structural "void" in which it is located. It can be seen that the valuesobtained for the activation energy associated with P_1 are lower than the values obtained for the dc process [34, 35] but close to those obtained for the ac conductivity [34, 35] which suggests a possible relation. Thus, the decrease in peak current P_1 with the increase in the heat treatment temperature is due to the reduction in the number of dipoles related to the decline in the number of ions structurally inserted in the glass network. The characteristic temperature of the current peak corresponds to the transition temperature from the non-equilibrium freezing state of the ions to the steady state, analogous to that occurring in the glasses with the glass transition temperature

[36]. The temperature shift of the TSDC peak P_1 with increasing heat treatment temperature can be justified based on the results of Agarwal [33] that associates it to the decrease in the number of network modifier ions.

In this type of glass containing alkaline ions a second depolarization peak can be detected, centered at higher temperatures and attributed to the dipolar depolarization coming from the movements of the electric charge transport units in limited paths, which result from the presence of micro-heterogeneities in the glass [33]. According to Hong, these movements are essentially associated with the jumps of the ions structurally inserted in the network, which is within the structural void in which they jump between different positions. Thus, the dipole formed between these ions and the non-bridging oxygen ion closest to each "free" ion, should present an activation energy higher than that associated with P_1. This motion is usually associated with a dc conductivity, giving rise to space-charge polarization. However, Agarwal et al. contend that this process must have an activation energy lower than the dc activation energy, which in this case is not verified [34, 35]. Thus, based on the values of the activation energy, the peak P2 is not assigned to space-charge depolarization but rather to the depolarization of the interfacial dipoles formed between the sample surface and the electrode. The decrease in the temperature at which peak P2 occurs with the rise of the heat treatment temperature may be related to the observed reduction in the dielectric loss factor [34, 35], which should indicate an increase in the number of dipoles. It is suggested that the presence of this current peak in the base glass sample should be detectable at temperatures above 400 K (maximum measurement limit). In addition to the P_2peak and with increasing temperature, an increase in current is observed in all samples. This current, usually referred to as background current, was adjusted by an Arrhenius expression to obtain the activation energy of this thermally activated process. It decreases with increasing heat treatment temperature indicating a greater mobility of the charge carriers in this temperature range.

Concerning the relaxation times, assuming that the value of τ calculated for each peak of depolarization current corresponds to the mean value of the relaxation times distribution, it is verified that the value of τ for P_1 (Table 14.1), displays a maximum for the base sample. We believe that this maximum may be associatedwith the fact that this sample has the highest number of ions structurally inserted in the network and, therefore, a broader distribution of relaxation times. The increase of τ related with P_1 from the sample treated at 600 to the sample treated at 650 °C, is related to the presence of $LiNbO_3$ crystals whose dipoles are difficult to depolarize resulting in a longer relaxation time. The decrease in the value of τ related toP_2, with the increase of the thermal treatment temperature, suggests that the dipoles that give rise to this depolarization are not linked to the presence of $LiNbO_3$ crystallites. Knowing that the density ratio between these crystals and the glass matrix increases and also that these crystals are difficult to depolarize, the relaxation time would otherwise greater than τ_{P1}. Thus, this relaxation time τ_{P2} should, as indicated, be associated with the depolarization produced by interfacial sample-electrode dipoles. The decrease in τ_{P2} with increasing heat treatment temperature is due to the decrease in the activation energy, which will facilitate the mobility and the return to equilibrium positions.

14.5   Conclusions

This contribution shows the principles of the thermally stimulated depolarization current method. The advantages and disadvantages are discussed; and present an example of the application of this electrical characterization technique applied to a glass and glass-ceramic samples is presented. The TSDC results of the $60SiO_2$-$30Li_2O$-$10Nb_2O_5$ glass composition, with and without heat-treatments reveal the presence of at least two thermally stimulated depolarization mechanisms. The depolarization peak current detected at lower temperatures (<250 K) is due to the depolarization of the dipoles associated with ions structurally inserted in a glass network. The second peak of depolarization, centered at temperatures >250 K, is due to the dipolar depolarization from the movements of the electric charge transport units in limited paths. The presence of depolarization current peaks at temperatures higher than the second peak should be associated with dipoles formed between the sample surface and the electrodes.

References

1. Bucci C, Fieschi R (1964) Ionic thermoconductivity. Method for the investigation of polarization in insulators. Phys Rev Lett 12(1):16–19
2. Chen R, Kirsh Y (1981) The analysis of thermally stimulated processes. Pergamon Press, New York
3. Carr SH (1982) Thermally stimulated discharge current analysis of polymers. In: Seanor DA (ed) Electrical properties of polymers. Academic, New York
4. Araujo EB, Abreu JAM, Oliveira RS, Paiva JAC, Sombra ASB (1997) Structure and electrical properties of lithium niobophosphate glasses. Can J Phys 75:747–758
5. Turnhout JV (1987) Thermally stimulated discharge of electrets. In: Sessler G (ed) Electrets. Springer, Berlin
6. Hong C, Day DE (1979) Thermally stimulated polarization and depolarization current (TSPC/ TSDC) techniques for studying ion motion in glass. J Mater 14:2493–2499
7. Milankovic AM, Day DE (1993) Thermally stimulated polarization and dc conduction in iron phosphate glasses. J Non-Cryst Solids 162(3):275–286
8. Hong C, Day DE (1981) Thermally stimulated currents in sodium silicate glasses. J Am Ceram Soc 64(2):61–68
9. Prezas PR, Melo BMG, Costa LC, Valente MA, Lança MC, Ventura JMG, Pinto LFV, Graça MPF (2017) TSDC and impedance spectroscopy measurements on hydroxyapatite, β-tricalcium phosphate and hydroxyapatite/β-tricalcium phosphate biphasic bioceramics. Appl Surf Sci 424 (1):28–38
10. Xu Y (1991) Ferroelectric materials and their applications. North-Holland
11. Fillard JP, Van Turnhout J (1977) Thermally stimulated processes in solids: new prospects. J Electrost 3:1–302
12. Horiuchi N, Nakamura M, Nagai A, Katayama K, Yamashita K (2012) Proton conduction related electrical dipole and space charge polarization in hydroxyapatite. J Appl Phys 112 (7):074901
13. Garlick GFJ, Gibson AF (1948) The electron trap mechanism of luminescence in sulphide and silicate phosphors. Proc Phys Soc 60(6):574–590

14. McKeever SWS, Hughes DM (1975) Thermally stimulated currents in dielectrics. J Phys D Appl Phys 8:1520–1529
15. Kristianpoller N, Kirsh Y (1979) Thermally stimulated depolarization currents in barium floride. J Phys C Solid State Phys 12(6):1073–1079
16. Paul A (1982) Chemistry of glasses. Chapman & Hall, London
17. James PF (1995) Glass-ceramics – new compositions and uses. J Non-Cryst Solids 181:1–15
18. Keding R, Rüssel C (1997) Electrochemical nucleation for the preparation of oriented glass ceramics. J Non-Cryst Solids 219:136–141
19. Shankar MV, Varma KBR (1999) Dielectric and optical properties of surface crystallized TeO2-LiNbO3 glasses. J Non-Cryst Solids 243:192–203
20. Jain H (2004) Transparent ferroelectric glass-ceramics. Ferroelectrics 306:111–127
21. Halliyal A, Bhalla AS, Newnham RE (1983) Polar glass-ceramics – a new family of electroceramic materials -tailoring the piezoelectric and pyroelectric properties. Mater Res Bull 18:1007–1019
22. Dan A, Chakravorty D (2000) Dielectric properties of silver in a glass-ceramic containing the lithium niobate phase. J Mater Res 15(6):1324–1330
23. Prassas M. Silica glass from aerogels. http://www.solgel.com/articles/april01/aerog2.htm
24. Ding Y, Miura Y, Nakaoka S, Nanba T (1999) Oriented surface crystallization of lithium niobate on glass and second harmonic generation. J Non-Cryst Solids 259:132–138
25. Aboulleil MM, Leonberger FJ (1988) Model for ion-exchanged wave-guides in glass. J Am Ceram Soc 71:497–502
26. Vogel EM (1989) Glasses as nonlinear photonic materials. J Am Ceram Soc 72:719–724
27. Weiss GH, Bendler JT, Dishon M (1985) Analysis of dielectric loss data using the williams-watts function. J Chem Phys 83–3:1424–1427
28. Haertling GH (1999) Ferroelectric ceramics: history and technology. J Am Ceram Soc 82(4):797–818
29. Prasad E, Sayer M, Vyas HM (1980) Li+ conductivity in lithium-niobate silica glasses. J Non-Cryst Solids 40:119–134
30. Todorovic M, Radonjic L (1997) Lithium-niobate ferroelectric material obtained by glass crystallization. Ceram Int 23:55–60
31. Agarwal AK, Day DE (1982) Thermally stimulated currents and alkali-ion motion in silicate glasses. J Am Ceram Soc 65(2):111–117
32. Hong C, Day DE (1981) Thermally stimulated currents in sodium-silicate glasses. J Am Ceram Soc 64(2):61–67
33. Agarwal AK, Day DE (1981) Polarization and conduction mechanism in mixed-alkali glasses. J Am Ceram Soc 65(5):231–237
34. Graca MPF, Ferreira da Silva MG, Valente MA (2007) Structural and electrical properties of SiO2-Li2O-Nb2O5 glass and glass-ceramics obtained by thermoelectric treatments. J Mater Sci 42:2543–2550
35. Graca MPF, Ferreira da Silva MG, Sombra ASB, Valente MA (2006) Study of the electric and dielectric properties of SiO2-Li2O-Nb2O5 solgel glass-ceramics. J Non-Cryst Solids 352:5199–5204
36. Doi A (1998) Comparison of frequency-domain and temperature-domain electrical responses of ion-conducting glass. Solid State Ionics 107:81–88